Spontaneous Formation of Complex Micelles from a Homogeneous Solution

Xuehao He[1] and Friederike Schmid[2]

[1]*Department of Polymer Science and Engineering, Tianjin University, 300072 Tianjin, China*
[2]*Fakultät für Physik, Universität Bielefeld, D-33615 Bielefeld, Germany*
(Received 19 December 2007; published 4 April 2008)

We present an extensive computer simulation study of structure formation in amphiphilic block copolymer solutions after a quench from a homogeneous state. By using a mesoscopic field-based simulation method, we are able to access time scales in the range of a second. A "phase diagram" of final structures is mapped out as a function of the concentration and solvent philicity of the copolymers. A rich spectrum of structures is observed, ranging from spherical and rodlike micelles and vesicles to toroidal and net-cage micelles. The dynamical pathways leading to these structures are analyzed in detail, and possible ways to control the structures are discussed briefly.

PACS numbers: 61.25.H−, 64.75.Yz, 83.10.Rs

Amphiphilic molecules in solution such as lipids or amphiphilic block copolymers self-assemble into a variety of structures, e.g., spherical or cylindrical micelles, lamellae, and vesicles [1]. In the case of single-component amphiphiles, vesicular and toroidal structures are energetically less favorable than lamellar and cylindrical structures due to the energy penalty for bending. Nevertheless, they may be stabilized by entropic or kinetic factors and still form spontaneously. These structures provide new opportunities for designing soft materials with enhanced functionalities for various applications, such as complex microrelease systems or templates for nanodevice fabrication [2–7]. A detailed understanding of the aggregation process is crucial to understand and eventually control their formation.

In the past decades, a number of experimental studies have revealed the rich diversity of micellar morphologies displayed by amphiphilic systems. Besides spherical, rodlike, or wormlike micelles, micelles with various special topologies have been observed, such as unilamellar and multilamellar vesicles, onion vesicles, genus vesicles [2–10], toroidal micelles with one or several rings, and net or cage micelles [11–14]. The experiments indicated that the micellar structures and size distributions not only depend on molecular parameters, i.e., the chain length of the amphiphilic molecules, the hydrophilic-to-hydrophobic ratio, the molecular stiffness, and the intermolecular interactions, but also on system parameters such as the concentration, and on kinetic factors such as the diffusion ability of the amphiphilic molecules and the details of the manufacturing process. Unfortunately, detailed dynamical information on the process of spontaneous micelle formation is scarce. Only a few groups have captured the process of spontaneous vesicle formation in solutions of amphiphile mixtures and proposed a possible pathway of vesicle formation [15–19].

According to this "standard" pathway (PC), the amphiphilic molecules first self-assemble into small spherical micelles, these then coalesce to rods, the rods transform themselves to bilayers, and finally, the bilayers bend around and close up to vesicles. The last two steps are driven by the rim energy of the bilayers. The mechanism has been confirmed by computer simulations of different coarse-grained models [20–25]. It clearly contributes to the formation of vesicles in amphiphilic systems. However, it cannot explain the existence of complex toroidal structures, since no force pushes rodlike micelles with two detached end caps to form rings, let alone cage structures. In a recent paper, we have reported the existence of an alternative pathway of vesicle formation in copolymer solutions [26] (PG). In this pathway, the micelles do not coalesce, but simply grow by attracting copolymers from the solution. Once a critical micelle size is exceeded, copolymers start to flip-flop such that the micelle core becomes solvent-philic ("semivesicle" state). Finally, solvent diffuses inside the core, and the semivesicle swells into a vesicle. The two pathways are illustrated in Fig. 1 (see below for simulation details). The pathway PG may provide a possible route to toroidal structures.

In this Letter, we report on an extensive systematic study of structure formation in a single-component amphiphilic
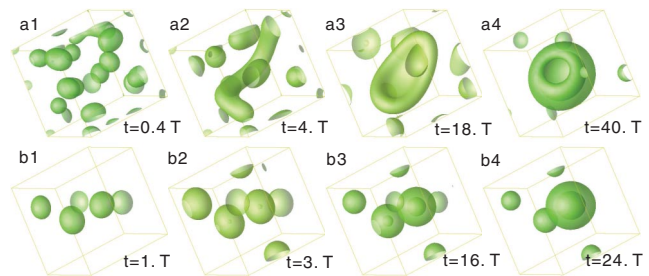
FIG. 1 (color online). Pathways of spontaneous vesicle formation in copolymer solutions. (a) PC: Micelle coalescence (a1),(a2), bilayer formation (a3), and bending (a4); (b) PG: micelle growth (b1),(b2), internal reorganization to semivesicle (b3), and swelling into vesicle (b4). The parameters of the simulations are $\chi_{BS} = 0.128$ and $\Phi_p = 0.2$, (a) $\Phi_P = 0.15$ (b). Times t are given in units of $T = 10^4 \tau_0$. Here and throughout the Letter, structure snapshots show isodensity surfaces of A blocks at $\Phi_A = 0.625$.

diblock copolymer system. The final self-assembled structures depend strongly on the copolymer concentration and the interaction parameters. By varying the latter over a wide range, we can map out the final topologies in a unifying "phase diagram." The simulations allow us to investigate the formation process in detail. Both pathways PC and PG described above can be observed, depending on the copolymer concentration. We find that vesicles and rodlike micelles may form irrespective of the pathway, but toroidal structures only form via the pathway PG. Our results thus demonstrate that complex structure formation is not only controlled by the molecular packing parameters, but also, crucially, by the details of the segregation kinetics.

Complex vesicle formation has also been studied recently by Sevink and Zvelindovsky [24,27]. They considered copolymers made of two incompatible blocks that were both basically solvent-phobic. As a result, the copolymers aggregated to compact, internally structured droplets (onion vesicles) with a relatively low solvent content (a few percent [27]). In contrast, in this work, we focus on copolymers with strongly solvent-philic components, and on open and hollow structures.

We consider a system of amphiphilic diblock copolymers P (copolymer volume fraction Φ_P) with solvent-phobic blocks A (chain fraction c_A) and solvent-philic blocks B (chain fraction $c_B = 1 - c_A$), immersed in a solvent S [28]. The monomer interactions are characterized in terms of Flory-Huggins parameters χ_{AB}, χ_{AS}, and χ_{BS}. A compressibility modulus κ_H ensures that the local density (polymer plus solvent) is roughly constant. The time evolution of the system is modeled with external potential dynamics [29], a dynamic density functional theory which locally conserves densities and is approximately valid for Rouse-type chain dynamics, but neglects hydrodynamics and reptation (see Ref. [26] for a compilation of the dynamical equations). The relevant dynamical model parameters are the mobility coefficients D_S and D_P of the solvent and the copolymer.

The parameter χ_{BS} and Φ_P were variable. The other model parameters were set to $\chi_{AB} = 0.896$, $\chi_{AS} = 1.024$, $\kappa_H = 1.176$, $c_B/c_A = 0.133$, and $D_S/D_P = 17$. The high values of χ_{AS} and χ_{AB} ensured that the A blocks segregate well from the B blocks and the solvent. Copolymers with short B blocks were used to stabilize bilayer structures in the regime where B is swollen with solvent. The remaining parameters, D_P and R_g (the unperturbed radius of gyration of the chains), set the length scale ($r_0 := R_g/3$) and the time scale ($\tau_0 := r_0^2/D_P$) of the simulation. Mapping these to real copolymer solutions such as, e.g., those studied in Ref. [30] ($D_P \approx 10^{-6}$ cm^2 s^{-1} and $R_g \approx 30$ nm), we find that our time unit corresponds to roughly $\tau_0 \sim 10^{-6}$ s.

On the technical side, the parameters of the simulation were as follows: The time step for integration of the dynamical equation was chosen $\Delta\tau = 0.02\tau_0$, on a spatial grid with grid size $r_0 = R_g/3$. The contours of the copolymer chains were discretized with $N = 17$ steps. A small

Gaussian noise was added to mimic the effect of thermal fluctuations [26]. The longest total simulation time was $7.2 \times 10^5 \tau_0$, corresponding to 0.72 s.

Figure 2 shows a diagram of final structures, obtained after quenching the system suddenly from an initially perfectly homogeneous state. The solvent philicity χ_{BS} ranges from positive to negative, in order to represent a wide class of amphiphilic block copolymers from nonionic to ionic. In addition, the copolymer volume fraction Φ_P was varied in the region where interesting structures were observed.

In order for structure formation to take place, the copolymer concentration Φ_P must exceed a certain critical value, which can be identified with the CMC (critical micelle concentration). At lower copolymer concentrations, the translational entropy of the copolymers prevents them from aggregating. The shape of the final structures depends on the solvent philicity of the B block, ($-\chi_{BS}$). At moderate χ_{BS} ($\chi_{BS} > 0$), the system favors bilayer structures and the copolymers aggregate to vesicles. As the solvent quality for the B block increases ($\chi_{BS} < 0$), the B block swells. Its radius R_B roughly scales with [31] $R_B \sim (c_B N)^{3/5}(1/2 - \chi_{BS})^{1/5}$ (N is the chain length). This in
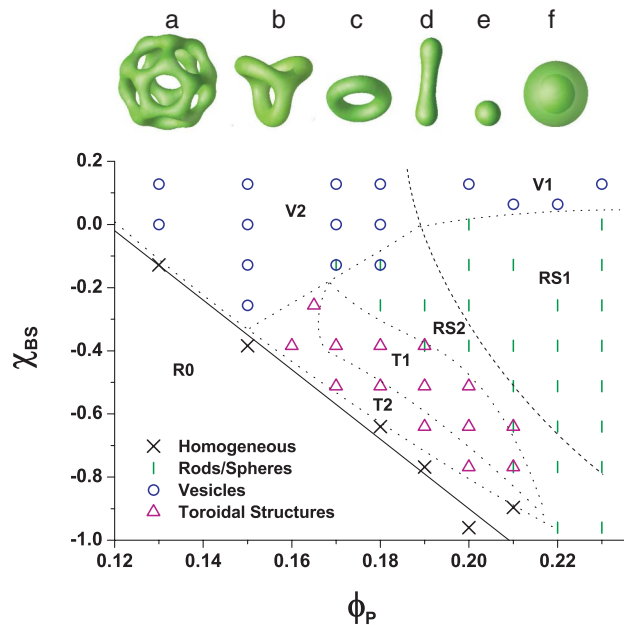
FIG. 2 (color online). "Phase diagram" of final structures after a sudden quench from an initially homogeneous copolymer solution, for a range of solvent-philicities χ_{BS} and copolymer volume fractions Φ_P. The final structures in the regions V1/V2 correspond to vesicles (f), RS1/RS2 to mixtures of rod and sphere micelles (d),(e), T1 to ring micelles (c), and T2 to toroidal micelles (a),(b). In the region R0, the solution stayed homogeneous. The dotted lines are guides for the eye. The dashed line separates two dynamical regimes where the structure formation proceeds along different pathways: Micelle coalescence (pathway PC) in the regions RS1 and V1, micelle growth (pathway PG) in the regions RS2, V2, T1, and T2. The solid line shows the function $\chi^* = 1.3 - 11.\Phi_P$ (see text and Fig. 4 for explanation).

turn decreases the critical packing parameter [1], the bilayers become unstable and give way to cylindrical and spherical structures. Consequently, the copolymers aggregate to rods and/or spheres in most of the parameter region. Close to the CMC, however, more complex structures are formed: Ring micelles, toroidal micelles, and even cage-like micelles.

To understand why these complex micelles appear, one must inspect the pathways of structure formation in more detail. Both pathways to vesicle formation, PC and PG, are observed in our system (Fig. 1). Likewise, rod formation also proceeds via the two distinct pathways micelle coalescence (PC), or (anisotropic) micelle growth (PG), depending on the copolymer volume fraction (Fig. 2): coalescence takes place at $\Phi_P > 0.2$. Rings and toroidal micelles emerge at much lower copolymer volume fraction, and their formation is clearly driven by a growth mechanism. Figure 3(a) shows the pathway to ring formation, where spherical micelles first grow into small disks, a hole then nucleates at the center of the disks, and finally, the perforated disks evolve into rings. Even closer to the CMC, the same mechanism leads to the formation of toroidal micelles: The micelles first grow into semivesicles or small vesicles, then several holes appear in the vesicle shells, until finally, the perforated vesicles grow into toroidal micelles [Figs. 3(b) and 3(c)]. The number of holes depends on the size of the embryo vesicle at the time of breakup. Close to the CMC, the dynamical stability of large vesicles increases: The initial number of micellar nuclei is small and they are far apart; hence, the vesicles are not perturbed by the environment and break up late. As a result, large cage micelles can be obtained in the vicinity of the CMC [Fig. 3(c)].

Next we examine the early stages of micelle aggregation. To this end, we define the segregation parameter $\sigma = \int dr |\Phi_A(r) + \Phi_B(r) - \Phi_P|/V$, where $\Phi_A(r)$ and $\Phi_B(r)$ are local monomer densities, and V is the volume. Looking at σ as a function of time, we find that the
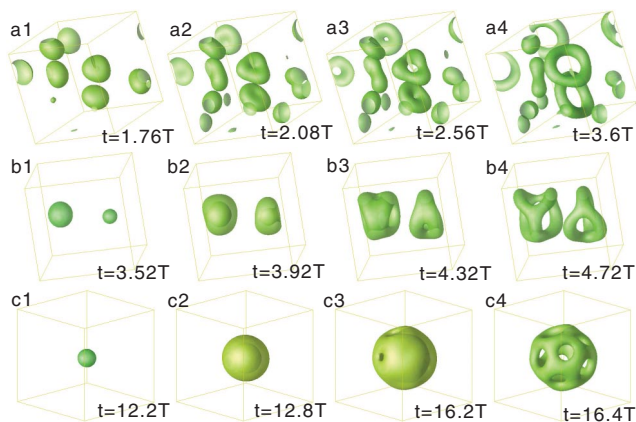
copolymer segregation proceeds in an almost steplike fashion after a well-defined "incubation time" τ^* (Fig. 4, inset). Figure 4 shows the incubation times as a function of χ_{BS} for different copolymer volume fractions Φ_P. Remarkably, most curves collapse onto a single power law function $1/\tau^* = A(\chi_{BS} - \chi^*)^\alpha$ with the exponent $\alpha \approx 1.25$ after a simple shift of χ_{BS} by $\chi^*(\Phi_P) = 1.3–11\Phi_P$. Only for the lowest copolymer volume fractions, $\Phi_P = 0.13$ and $\Phi_P = 0.15$, do the data fail to collapse; however, the slopes of these curves, shifted by χ^* and plotted in a double logarithmic way, are still comparable to α.

A similar power law behavior has been observed previously in a simulation study of vesicle formation in two dimensions [26]. It was explained in terms of the Cahn-Hilliard theory for spinodal decomposition, and χ^* was identified with the spinodal for macrophase separation between polymer and solvent. In the present case, however, $\chi^*(\Phi_P)$ is significantly lower than that spinodal [32], it seems rather related to the CMC (cf. Fig. 2). It is worth noting that data collapse and power law behavior is observed in a range of Φ_P *regardless* of the final structure and the dynamical pathway of structure formation. This suggests that the characteristics of the initial stage of segregation are universal and related to a spinodal-type instability.

Once created, the micelles grow by attracting copolymers from the solution. In the pathway PC, the growth is supplemented by micelle coalescence. The question arises under which conditions this happens. In fact, most fusion events take place at early times [see Figs. 1(a1) and 1(a2)]. At later stages, they are impeded by two factors: The formation of a well-segregated, swollen *B*-corona at the surface of the micelles, and the emerging copolymer depletion zone around the micelles. Hence the density of micelle nuclei at the early stage is a candidate quantity that might select between pathways. The crossover be-

FIG. 3 (color online). Formation of toroidal structures at $\chi_{BS} = -0.512$: (a) rings ($\Phi_P = 0.2$), (b) toroidal micelles ($\Phi_P = 0.18$), (c) cage micelles ($\Phi_P = 0.17$). Times t are given in units of $T = 10^4 \tau_0$.
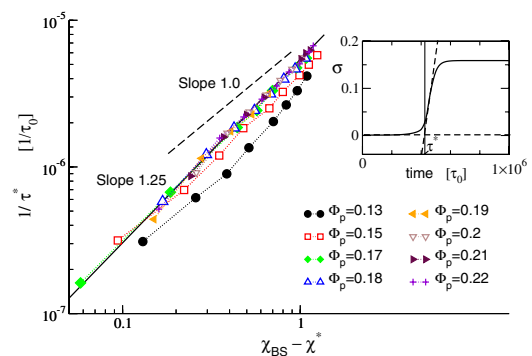
FIG. 4 (color online). Inverse incubation time $1/\tau^*$ as a function of χ_{BS} for different copolymer volume fractions χ^* as indicated. The values χ_{BS} have been shifted by $\chi^* = 1.3–11\Phi_P$. The solid line corresponds to the function $y = 5.3 \times 10^{-6}x^{1.25}$, and the dashed line shows $y \propto x^{-1}$ for comparison. Inset: Evolution of the order parameter σ with time at $\chi_{BS} = 0$, $\Phi_P = 0.17$. The incubation time is defined as the time where the tangent of $\sigma(t)$ at the inflection point and the base line $\sigma \equiv 0$ intersect each other.

tween pathways is observed at the copolymer volume fraction $\Phi_P \approx 0.2$. Taking into account that a large fraction of copolymers assembles into droplets almost simultaneously (at the time τ^*), and that these droplet nuclei roughly have the diameter $2R_g$, we can estimate the average distance D between droplets at given copolymer content [33] via $(2R_g/D)^3 \sim \Phi_P$. At $\Phi_P = 0.2$, D is of the order R_g. Hence the copolymers in solution are in contact with several droplets, they are attracted by all of them, and can serve as bridges that mediate fusion.

In the last stage, the structures ripen. As long as they are still small (semivesicle state), classical Oswald coarsening is observed [Figs. 1(a3), 1(a4), 1(b3), and 1(b4)]: Small structures dissolve, large structures grow, driven by the competition of bulk and surface free energy. Once the structures have locally assumed their favored toroidal or bilayer structure, the Oswald process stops and the ripening is governed by much weaker thermodynamic forces, such as, e.g., those associated with the bending energy. The time scales of these processes are very slow and out of reach for our simulation method. Therefore, we have carried out a set of simulations using external potential dynamics with locally nonconserved (but globally conserved) densities. This dynamical model is less realistic, but much faster, such that we could also assess later stages of the aging process. Specifically, we studied the evolution of a system containing two vesicles with different initial sizes in two and in three dimensions. In the case of ring micelles or two dimensional vesicles, the contribution of the bending energy favors a uniform size distribution: The energy of a single ring of radius R is proportional to k/R (k being the bending rigidity), and the total energy for a fixed number of rings is minimal if all rings have the same diameter. Indeed, our two dimensional simulations showed that the sizes of the two rings converged in the course of the simulation: The small ring grew at the expense of the large ring. For three dimensional vesicles, the situation is different: The bending energy of a vesicle is $4\pi k$, independent of its size. The total bending energy only depends on the number of vesicles, not on their size distribution. Consequently, we did not observe any sign of size uniformization, nor size disproportionation, in the three dimensional simulations. The same behavior has been observed in experiments [34].

To summarize, we have investigated the formation of toroidal micelles in copolymer solutions, and shown that such micelles may form in the vicinity of the CMC by a pathway that proceeds via the nucleation, growth, and subsequent breakup of vesicles. The competition of copolymer aggregation and self-assembly generates a kinetic trap that opens a route to manufacturing highly complex metastable structures. Several methods to control these kinetic traps are conceivable: Controlling the number of initial nuclei by planting seeds (prenucleation) [35,36], quenching from different initial states (e.g., quenching from a vesicle state), doping with additional components to tune the bilayer properties, or working with amphiphilic mixtures.

[1] J. Israelachvili, *Intermolecular and Surface Forces* (Academic Press, New York, 1991).
[2] H. Shen and A. Eisenberg, Angew. Chem. **39**, 3310 (2000).
[3] J. Zipfel *et al.*, Macromolecules **35**, 4064 (2002).
[4] L. F. Zhang and A. Eisenberg, Macromolecules **29**, 8805 (1996).
[5] L. F. Zhang, K. Yu, and A. Eisenberg, Science **272**, 1777 (1996).
[6] K. Yu, C. Bartels, and A. Eisenberg, Langmuir **15**, 7157 (1999).
[7] K. Yu and A. Eisenberg, Macromolecules **31**, 3509 (1998).
[8] J. Z. Du and Y. M. Chen, Angew. Chem. **116**, 5194 (2004).
[9] Y. Y. He *et al.*, J. Am. Chem. Soc. **128**, 2745 (2006).
[10] J. H. Lee *et al.*, Phys. Rev. Lett. **96**, 048102 (2006).
[11] I. C. Reynhout, J. J. L. M. Cornelissen, and R. J. M. Nolte, J. Am. Chem. Soc. **129**, 2327 (2007).
[12] Y. Jiang *et al.*, J. Phys. Chem. **109**, 21 549 (2005).
[13] S. Jain and F. S. Bates, Science **300**, 460 (2003).
[14] D. J. Pochan *et al.*, Science **306**, 94 (2004).
[15] S. U. Egelhaaf and P. Schurtenberger, Phys. Rev. Lett. **82**, 2804 (1999).
[16] T. M. Weiss *et al.*, Phys. Rev. Lett. **94**, 038303 (2005).
[17] S. Schmölzer *et al.*, Phys. Rev. Lett. **88**, 258301 (2002).
[18] M.-P. Nieh *et al.*, Langmuir **21**, 6656 (2005).
[19] J. Leng, S. U. Egelhaaf, and M. E. Cates, Europhys. Lett. **59**, 311 (2002).
[20] A. Bernardes, Langmuir **12**, 5763 (1996).
[21] H. Noguchi and M. Takasu, Phys. Rev. E **64**, 041913 (2001).
[22] S. Yamamoto, Y. Maruyama, and S.-A. Hyodo, J. Chem. Phys. **116**, 5842 (2002).
[23] A. H. de Vries, A. E. Mark, and S.-J. Marrink, J. Am. Chem. Soc. **126**, 4488 (2004).
[24] G. J. A. Sevink and A. V. Zvelindovsky, Macromolecules **38**, 7502 (2005).
[25] T. Uneyama, J. Chem. Phys. **126**, 114902 (2007).
[26] X. H. He and F. Schmid, Macromolecules **39**, 2654 (2006).
[27] G. J. A. Sevink and A. V. Zvelindovsky, Mol. Simul. **33**, 405 (2007).
[28] X. H. He *et al.*, J. Phys. Chem. B **108**, 1731 (2004).
[29] N. M. Maurits and J. G. E. M. Fraaije, J. Chem. Phys. **107**, 5879 (1997).
[30] I. C. Riegel *et al.*, Pure Appl. Chem. **76**, 123 (2004).
[31] P. G. de Gennes, *Scaling Concepts in Polymer Physics* (Cornell University Press, Ithaca, NY, 1979).
[32] The spinodal line is given by [26] $\chi_{BS}^{sp} = \chi_{AB}c_A - \chi_{AS}c_A/c_B + 1/(2c_B(1 - \Phi_P)) + 1/(2c_B N\Phi_P)$.
[33] Here we have neglected all other factors that might influence the droplet density, such as, e.g., an underlying fluid structure at the time τ^* [26].
[34] Z. Cheng and P. L. Luisi, J. Phys. Chem. B **107**, 10 940 (2003).
[35] J. G. E. M. Fraaije and G. J. A. Sevink, Macromolecules **36**, 7891 (2003).
[36] X. H. He and F. Schmid, Macromolecules **39**, 8908 (2006).